



INFLUENCE OF HORIZONTAL HEAT-INSULATING PLATES ON THE STRUCTURE OF CONVECTIVE FLOWS AND HEAT TRANSFER IN A CLOSED CAVITY

A.Yu. Vasiliev, A.N. Sukhanovskii, P.G. Frick

Institute of Continuous Media Mechanics UB RAS, Perm, Russian Federation

The influence of horizontal insulating plates of different sizes on the structure of a convective flow and on the total heat flux in a cavity with aspect ratio 5 is studied numerically. Direct numerical simulations have been performed using the open source software OpenFoam 4.1 at Prandtl number 6.12 and for two Rayleigh numbers: $3.9 \cdot 10^7$ and $3.9 \cdot 10^8$. In all calculations the plates are of the same thickness. It is found that the location and size of the plate strongly influence the structure of the flow. Changes in the mean flow structure have little effect on the heat flux in the case of a small plate. An increase in the size of the plate leads to little change in the heat flux, except for the case when the plate is located near the lower boundary. In this case, the Nusselt number is 25% less compared to Rayleigh–Bénard convection. It is found that the values of kinetic energy and Nusselt number do not correlate with each other. As the Rayleigh number increases, the influence of the plate on the heat flux decreases. It is shown that an insulating plate has no significant effect on the heat flux if the height of the plate location is significantly larger (10 times or more) than the thickness of the temperature boundary layer. It has been established that the presence of plates in the fluid volume significantly affects the integral values of velocity and temperature fluctuations.

Key words: turbulent convection, heat flux, boundary layer, numerical simulation

1. Introduction

Free thermogravitational convection determines intensity and structure of fluid flows in various natural and technological systems [1,2]. Dynamics and structure of convective flows are extremely various and essentially depend on geometrical parameters of system, boundary and initial conditions [3-7]. Particular attention is paid to the problem of heat transfer in the presence of convection, since the convective transfer may significantly exceed the heat transfer by conduction. At the same time, the influence of insulating bodies, floating or stationary, in the fluid volume, on the heat and mass transfer has been relatively poorly studied.

A surge of interest in the study of free-floating insulating bodies was caused by the problem of tectonic plate drift due to convection in the mantle of the planets [8]. The first models of continental drift and their interaction with currents in the mantle appeared in the late 80s of XX century [9]. Numerical simulations of continental drift and their influence on the formation of thermal plumes have been developed in [10-13], and significant progress in development of mathematical models of continental motion has been achieved by Russian scientists [14-17].

The first successful attempts at laboratory modeling of convection in the asthenosphere were realized in the case of fixed thermally insulated surfaces [18-20]. The interaction of insulating bodies and convection in the mantle implies the possibility of displacement of bodies under the action of viscous stresses on the liquid side. The dynamics of motion of an insulating plate floating freely on the surface of a layer heated from below and cooled from above is studied in [21], where it is shown that the plate motion is oscillatory. A more complicated case is considered in [22], where the insulating plate is immersed to different depths. In [23-25], it was demonstrated that the presence or absence of oscillations during the plate motion is determined by its size. In [25], a simple one-dimensional phenomenological model describing the plate dynamics is proposed. The effect on convective flow of a large number of small spherical-shaped bodies with low thermal conductivity and a density slightly higher than the liquid density is considered in [26]. Spherical bodies entrained by the flow concentrate in different areas on the lower heat exchanger, which leads to a change in the direction of large-scale circulation. The dynamics of an insulating plate with different boundary conditions (constant temperature or zero heat flow) in a two-dimensional fluid flow with infinite Prandtl number value was investigated numerically in [27-29]. Both regular and chaotic modes were

found, which agrees with the experiment and confirms that complex dynamics is a characteristic feature of such systems.

The important issue of the influence of insulating plates on the heat transfer has been studied much less. Thus, the spatial arrangement of the insulating regions at the upper (cold) boundary and the corresponding value of the convective heat flux were analyzed in [30-32]. The results obtained turned out to be ambiguous. In [30], where large insulated regions were considered, it was shown that the integral heat flux is defined by the plate area and is weakly related to their location. On the contrary, in [31, 32] it was obtained that the frequency of spatial arrangement of insulating regions, while preserving their area, significantly changes the heat transfer: as the frequency increases, it approaches the value characteristic of an isothermal boundary. Convective heat transfer in the case of localized heating at the lower boundary was studied in [33, 34], where it was revealed that if the size of the heated region appreciably exceeds the thickness of the temperature boundary layer, the Nusselt number (ratio of total heat flux to the heat conductive flux) depends on the Rayleigh number to a degree close to 1/3. The study of convection in a cavity with inhomogeneous (including fractal) distribution of heating on the bottom (see [35, 36]) has revealed that the spatial distribution of heating elements at a fixed integral heating area significantly affects the structure of the flow and the value of heat flux. The presence of heat-insulating regions at both the upper and lower boundaries also significantly changes the structure of the flow [37].

The problem of heat transfer, which is crucial for natural and technological systems, in the case when thermal insulating bodies are located in the fluid volume, has almost not been studied. We can only mention the work [38], in which a set of vertical heat insulating plates, serving to destroy the main large-scale flow is considered. The main result was unexpected; it is shown that the presence of the plates suppresses the large-scale circulation, but practically does not change the thickness of the temperature boundary layer and the value of the heat flux.

Thus, most studies of convection with stationary or moving insulating bodies describe the case when the body is located on the upper or lower boundary. In this paper, we consider the influence of spatial arrangement of fixed horizontal insulating plate of different size, placed in the volume of liquid, on the formation of convective flows and the value of heat flux.

2. Statement of the problem and numerical simulation

Direct numerical simulation of turbulent convection in a rectangular cavity with an insulating plate was performed using the freely distributed open-source computational fluid dynamics package OpenFoam 4.1. The dimensionless system of equations describing the convective flow of a Newtonian incompressible fluid in the Boussinesq approximation was as follows:

$$\begin{aligned} \nabla \cdot \mathbf{u} &= 0, \\ \frac{\partial \mathbf{u}}{\partial t} + (\mathbf{u} \cdot \nabla) \mathbf{u} &= -\nabla p + \sqrt{\text{Pr}/\text{Ra}} \nabla^2 \mathbf{u} + \theta \mathbf{e}_y, \\ \frac{\partial \theta}{\partial t} + (\mathbf{u} \cdot \nabla) \theta &= \sqrt{\frac{1}{\text{Ra Pr}}} \nabla^2 \theta, \end{aligned} \quad (1)$$

where $\mathbf{u} = u\mathbf{e}_x + w\mathbf{e}_y$ — velocity vector, p — pressure, Ra and Pr — Rayleigh and Prandtl numbers, $\theta = (T - T_-)/\Delta T$ — temperature, $\mathbf{e}_x, \mathbf{e}_y$ — unit vectors in the direction of the x and y axes, respectively. As measurement units for the dimensionless equations of thermogravitational convection (1) were chosen: the height of the fluid layer H ; velocity $u_f = \sqrt{g\beta\Delta H}$; time $t_f = H/u_f$; temperature difference $\Delta = T_+ - T_-$ between hot (T_+) and cold (T_-) boundaries. The Rayleigh and Prandtl numbers were defined as

$$Ra = \frac{g\beta\Delta H^3}{\nu\chi}, \quad Pr = \frac{\nu}{\chi},$$

where ν — kinematic viscosity, χ — thermal diffusivity, β — thermal expansion coefficient, g — acceleration of gravity.

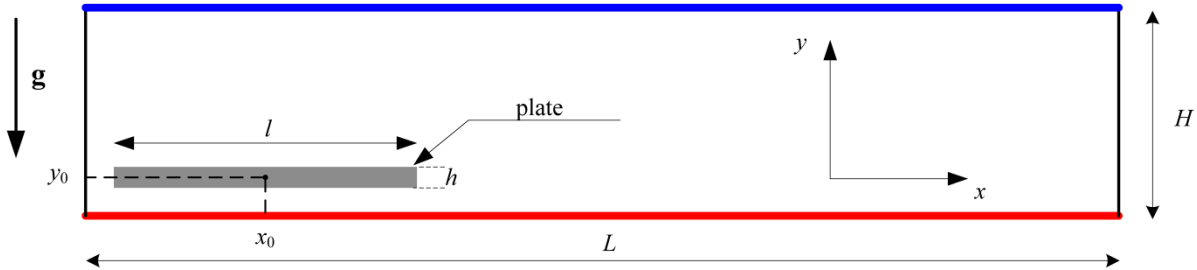


Fig. 1. Scheme of the computational domain and coordinate system.

Two-dimensional numerical simulation of convective turbulence in the case of a non-moving insulating plate is performed for a fixed value of Prandtl number $Pr = 6,12$, aspect ratio $\Gamma = L/H = 5$ and two values of Rayleigh number: $Ra = 3,9 \cdot 10^7$ and $Ra = 3,9 \cdot 10^8$. The scheme of the studied area is shown in Figure 1. The purpose of the calculations was to study the effect of the heat-insulating plate on the flow structure and heat transfer. Two plates in the form of rectangles of the same height $h = 0,02$, but different length: $A = l/L \approx 1/6$ и $A = 1/2$ are considered. The position of the plate in the computational domain was characterized by the coordinates of the center of mass (x_0, y_0) .

No-slip boundary condition ($\mathbf{u} = 0$) is used for cavity boundaries and surface of the plate. The side walls of the cavity are adiabatic: $\partial\theta/\partial n = 0$ and upper and lower boundaries are isothermal: $\theta = 0$ and $\theta = 1$.

The analysis of the convergence of the numerical solution was performed for the largest value of the Rayleigh number on grids with the total number of control volumes (CV) $N = 0,64 \cdot 10^6$; 10^6 ; $1,44 \cdot 10^6$. Comparison of integral Nusselt numbers $Nu = 1 + \sqrt{Ra Pr} \langle w\theta \rangle_{s,t}$, obtained for different grids, showed that values of Nu change very weakly (less than 1%) at $N > 10^6$. Here $\langle \cdot \rangle_s$ describes averaging over the whole domain. All calculations presented in the paper were performed on a multiblock structured grid with $N = 10^6$. Table 1 shows the parameters of the computational grid and the coordinates of the center of mass of the plates, for which the calculations were performed.

Table 1. Parameters of the computational grid and coordinates of the center of mass of the insulating plate (x_0, y_0) .

Ra	A	Δ/η_K	Δ/η_B	N_x^0	N_x''	N_y^0	N_y''	(x_0, y_0)		
$3,7 \cdot 10^7$	1/6	0,15	0,38	5/3	9/3	23/3	43/3	(0,625, 1/8)	(1,25, 1/8)	(2,5, 1/8)
								(0,625, 1/4)	(1,25, 1/4)	(2,5, 1/4)
								(0,625, 1/2)	(1,25, 1/2)	(2,5, 1/2)
	1/2	0,15	0,38	5/3	9/3	23/3	43/3	(1,37, 1/8)		(2,5, 1/8)
								(1,37, 1/4)		(2,5, 1/4)
								(1,37, 1/2)		(2,5, 1/2)
$3,7 \cdot 10^8$	1/2	0,31	0,77	4/4	5/4	13/4	25/4	(1,37, 1/8)		(2,5, 1/8)

The number of CV in the boundary layers (dynamic — N'' , and thermal — N^0) satisfied the estimate of their minimum quantity proposed in [39]. Direct numerical modeling assumes that the

applied grid must resolve the Kolmogorov scale $\eta_K = H \text{Pr}^{1/2} / (\text{Ra}(\text{Nu}-1))^{1/4}$ and Batchelor scale $\eta_B = \eta_K \text{Pr}^{-1/2} = H / (\text{Ra}(\text{Nu}-1))^{1/4}$.

In all calculations, the maximum average size of CV $\Delta = (\Delta_x \Delta_y)^{1/2}$ did not exceed the scale of Kolmogorov and Batchelor. The equations of thermogravitational convection were solved using a standard solver *buoyantBoussinesqPimpleFoam*. The time integration was carried out according to the implicit Euler scheme of the second order of accuracy. To discretize the convective and diffusive terms, a second-order central difference approximation scheme was used (in OpenFoam this scheme is called Gauss linear). To solve the system of linear algebraic equations obtained after discretization of the system of equations (1), we used the PBiCG bisector gradient method with the DILU preconditioner (for velocity and temperature) and the GAMG method (for pressure).

3. Results

3.1. Rayleigh-Benard convection

The basic case, with which the calculation results in the presence of insulating plates are compared, is Rayleigh-Benard convection with homogeneous boundary conditions of the first kind at the upper and lower boundaries. At $\text{Ra} = 3,9 \cdot 10^7$ the mean flow is asymmetrical and represents 5 rolls of different sizes, each of which rotates in the opposite direction compared to its neighbors (Fig. 2a). It should be noted that for a layer with aspect ratio $\Gamma = 8$ ($\text{Ra} = 10^6$, $\text{Pr} = \infty$) in the presence of a small plate floating on the fluid surface, i.e., weakly affecting the structure of the currents, the average flow consists of five rolls [27]. Thus, the main flow in the form of several rolls is characteristic of Rayleigh-Benard convection in cavities with a large aspect ratio in developed regimes. In our study, an increase in the Rayleigh number to $\text{Ra} = 3,9 \cdot 10^8$ changes the flow structure to a four-roll structure (Fig. 2b).

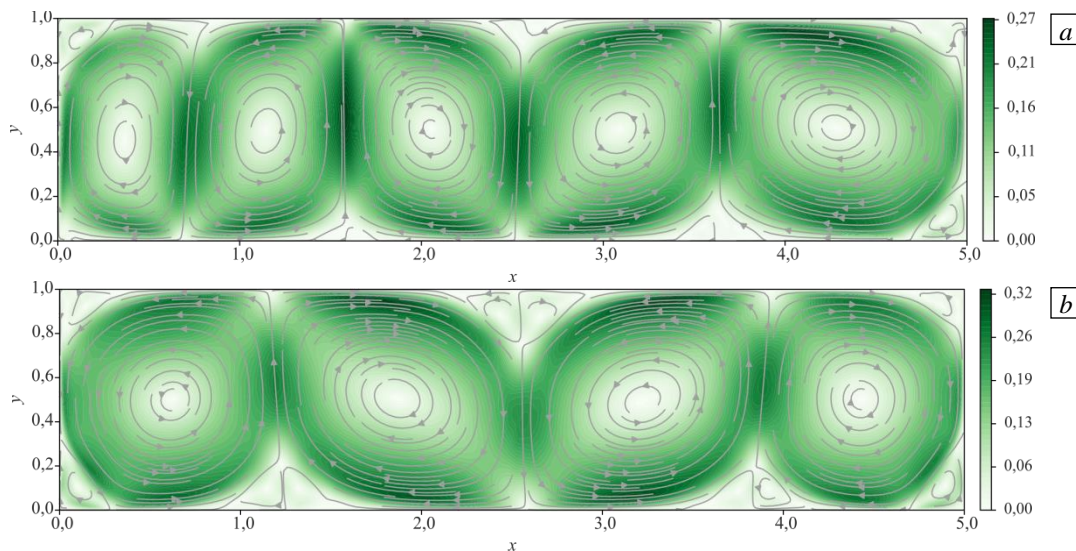


Fig. 2. Streamlines of time-averaged velocity fields at $\text{Ra} = 3,9 \cdot 10^7$ (a) and $\text{Ra} = 3,9 \cdot 10^8$ (b); velocity magnitude is shown in color.

The decomposition of the instantaneous velocity fields into spatial modes makes it possible to isolate the main modes of the flow and to understand the cause of asymmetry of the mean flow at a low Rayleigh number. For this purpose, we used a decomposition into Fourier modes by free-slip basis functions [7], which shows its efficiency for studying the dynamics of large-scale circulation in two-dimensional and quasi-two-dimensional formulations [37, 40]. In spite of the fact that the basis functions do not satisfy the non-slip condition at solid boundaries, they adequately describe the flow

structure and make it possible to determine the modes with the highest energy, which is confirmed by the results of POD (Proper Orthogonal Decomposition) analysis [41, 42]. The decomposition has the form:

$$u(x, y, t) = (4/5) \sum_n A_{n,1}^x(t) \sin(\pi n x / 5) \cos(\pi y),$$

$$w(x, y, t) = (4/5) \sum_n A_{n,1}^y(t) \cos(\pi n x / 5) \sin(\pi y), \quad n \in \{1, 7\},$$

$$E_n = (1/2) \left\langle A_{n,1}^x(t)^2 + A_{n,1}^y(t)^2 \right\rangle_t,$$

where $\langle \cdot \rangle_t$ defines time averaging. Figures 3a, b shows the energy of the seven lower modes of flow for two values of the Rayleigh number. It can be seen that in the case of $Ra = 3,9 \cdot 10^7$, flow is formed as a result of the superposition of the three modes, while for $Ra = 3,9 \cdot 10^8$, there is a single-mode flow. The temporal evolution of the basic modes for $Ra = 3,9 \cdot 10^7$ is presented in Fig. 3c. The three main modes coexist during the entire analyzed time interval, with their amplitudes varying appreciably in a non-periodic manner.

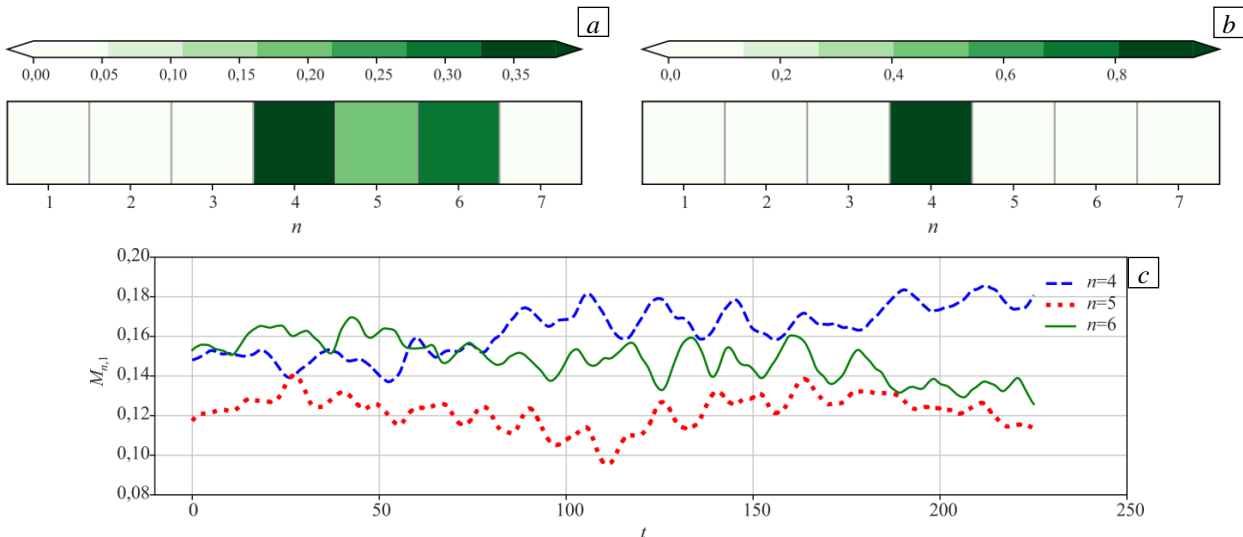


Fig. 3. Time-averaged normalized energy of the main modes $E_n / \sum_n E_n$ at $Ra = 3,9 \cdot 10^7$ (a) and

$Ra = 3,9 \cdot 10^8$ (b); temporal evolution of the amplitudes of the most energetic modes

$$M_{n,1} = \sqrt{A_{n,1}^x(t)^2 + A_{n,1}^y(t)^2} \quad \text{at } Ra = 3,9 \cdot 10^7 \text{ (c)}.$$

Figure 4 shows the distribution of the rms (*root mean square*) temperature pulsations $\delta\theta_{rms} = \sqrt{\left\langle (\theta - \langle \theta \rangle_t)^2 \right\rangle_t}$ and turbulent kinetic energy $k = (1/2) (\delta u_{rms}^2 + \delta w_{rms}^2)$ in the cavity. The largest pulsations are concentrated in the regions of vertical flows formation (in the places of ascending/descending of thermal plumes), with the temperature pulsations being maximal in the area of plume breakup, and the velocity pulsations - at the opposite boundary, where the accelerated plume hits the boundary. The ascent of a thermal plume leads to destruction of the thermal boundary layer, which requires some characteristic time to recover. Then a new thermal plume is formed and detached, and the process is repeated.

The average kinetic energy $E_k = (1/2) \left\langle |\mathbf{u}_i|^2 \right\rangle_{s,t}$, energy of turbulent pulsations $\langle k \rangle_s$, energy of temperature pulsations $k_\theta = \langle \delta\theta_{rms}^2 \rangle_s$ and integral Nusselt number are used as integral characteristics of the convective system. The values of the integral characteristics for the two regimes of Rayleigh-

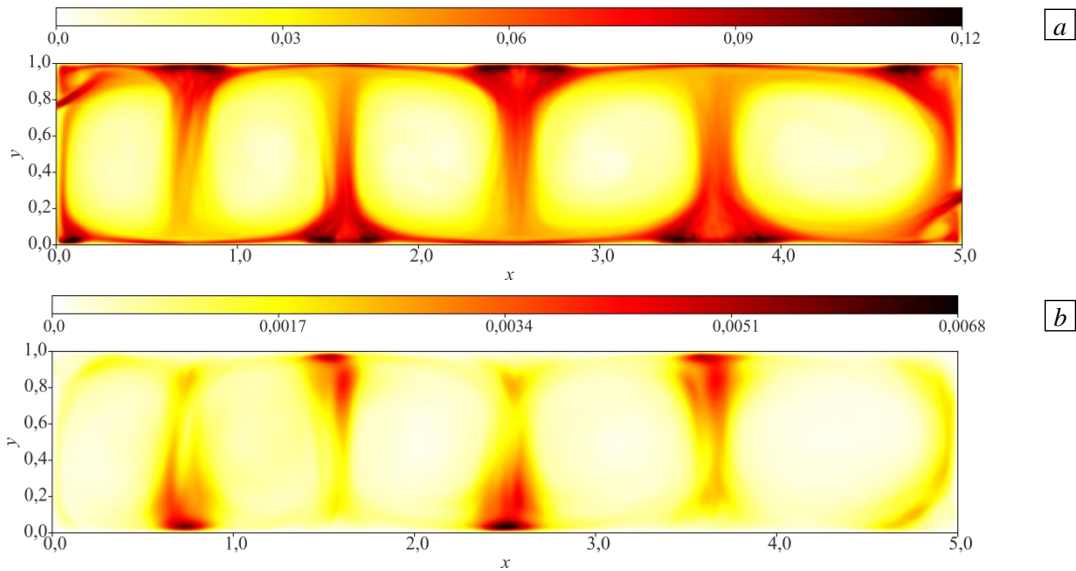


Fig. 4. Distribution of the rms temperature pulsations $\delta\theta_{rms}$ (a) and turbulent kinetic energy k (b), $Ra = 3,9 \cdot 10^7$.

Benard convection are presented in Table 2. An increase in the Rayleigh number by an order of magnitude leads to an almost twofold increase in the Nusselt number (by 77%). At the same time, the other integral characteristics change much weaker. Somewhat unexpected was the observed decrease in the level of temperature pulsations with an increase in the Rayleigh number (by 31%). In this case, this is a consequence of the transition to a more stable single-mode flow.

Table 2. Values of integral characteristics in Rayleigh-Benard convection.

Ra	Nu	$E_k \cdot 10^3$	$\langle k \rangle_S \cdot 10^3$	$k_\theta \cdot 10^3$
$3,9 \cdot 10^7$	21,3	10,5	0,91	1,67
$3,9 \cdot 10^8$	37,9	13,9	0,10	1,15

3.2. Convection in the case of a small plate $A \approx 1/6$ (case I)

The effect on convection in the cavity of a relatively small fixed heat insulating plate ($A \approx 1/6$) is considered. The calculations were performed for different vertical and horizontal positions of the plate. Figure 5 illustrates the structure of the convective flow for the nine investigated configurations of the computational domain and shows that the plate position significantly affects the structure of the mean flow, namely, the number and shape of convective rolls change. Here and below in the text, the heat-insulating plate is indicated in black in the figures.

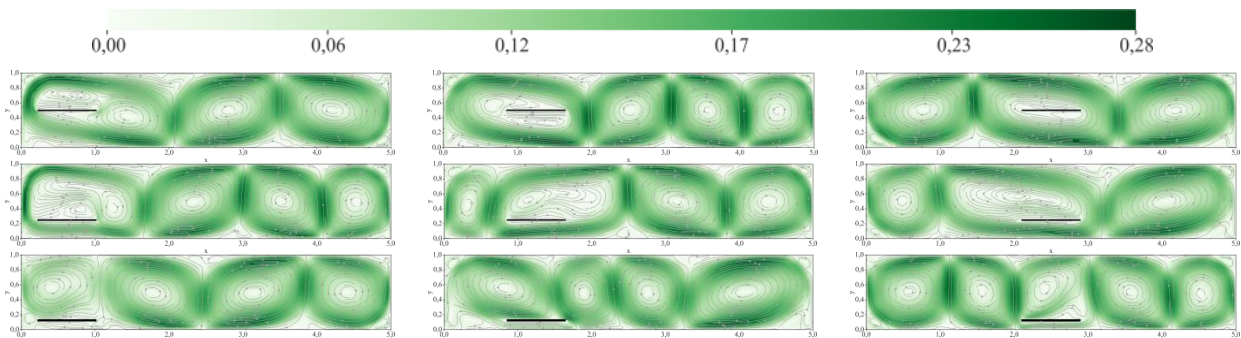


Fig. 5. The structure of the middle flow at different locations of the heat-insulating plate, $Ra = 3,9 \cdot 10^7$.

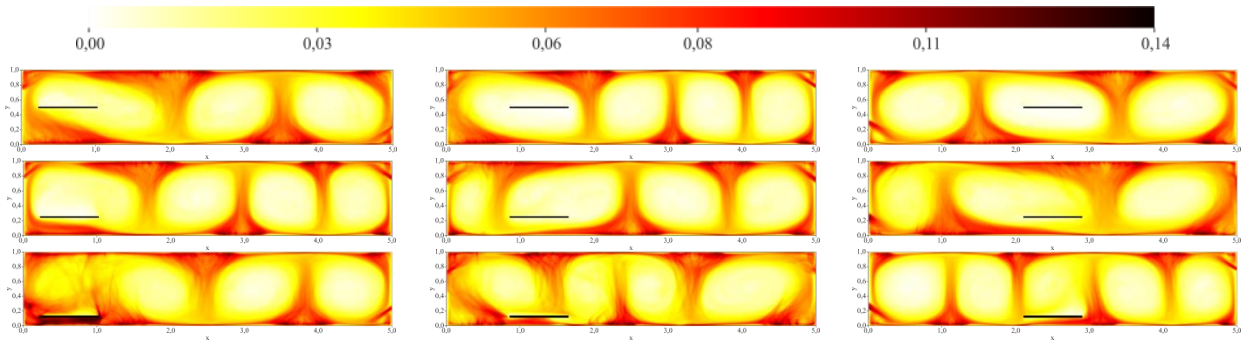


Fig. 6. Distribution of the rms temperature pulsations $\Delta\theta_{rms}$ with different location of the heat insulating plate, $Ra = 3,9 \cdot 10^7$.

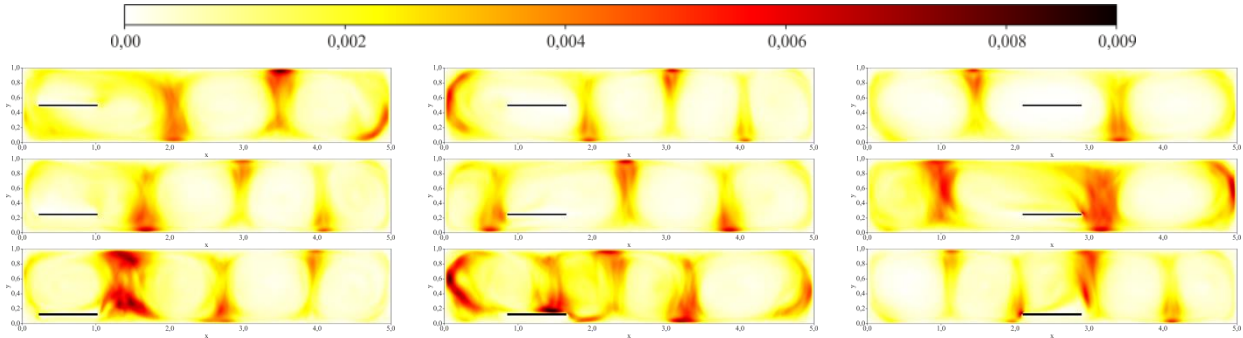


Fig. 7. Distribution of kinetic energy of turbulent pulsations k at different location of the heat insulating plate, $Ra = 3,9 \cdot 10^7$.

The plate introduced into the flow changes the location of the rising and sinking jets, and as a consequence, the areas with high levels of temperature and velocity pulsations (Fig. 6, 7). Spatial distribution of pulsations depends on the location of the plate. In the case of $x_0 = 1,25$, $y_0 = 0,125$ (see middle panels in the bottom row in Fig. 6, 7), the plate is on the way of the descending jet and concentrates velocity pulsations on its surface, while in case of $x_0 = 0,65$, $y_0 = 0,125$ (left bottom panels), the ascending jet is formed near the edge of the plate, and the highest velocity pulsations are seen precisely in this jet, both in the lower and in upper zones.

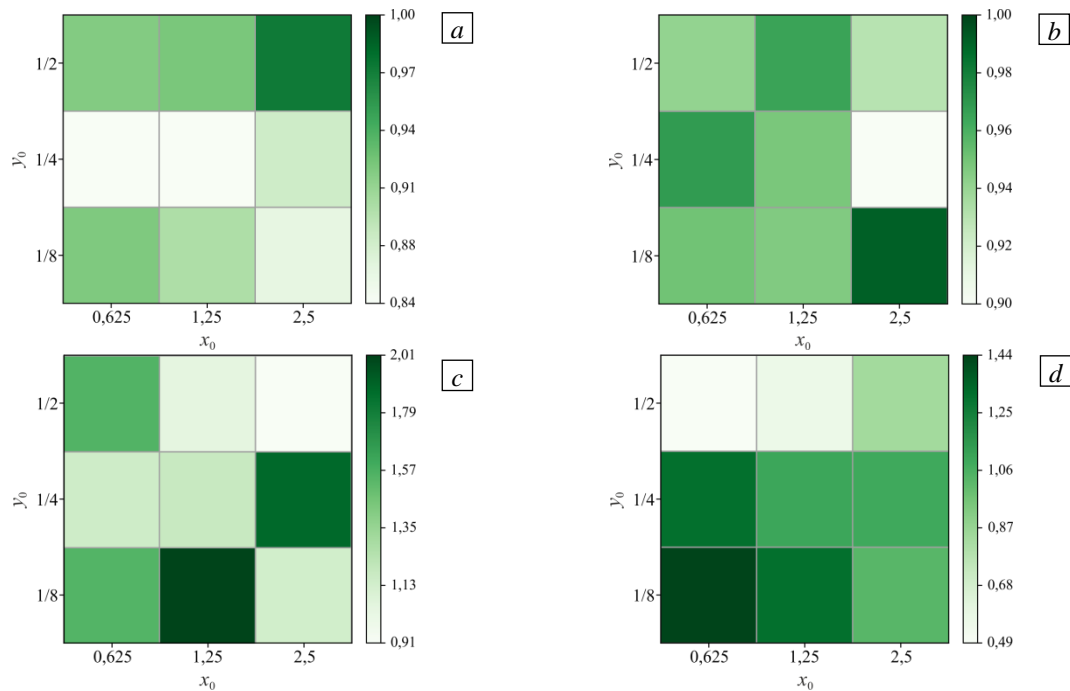


Fig. 8. Normalized integral values for all locations of the insulating plate at $Ra = 3,9 \cdot 10^7$: E_k^* (a), Nu_k^* (b), k^* (c) and k_0^* (d).

An important issue is the effect of the horizontal insulating plate on the integral characteristics of the flow. Figure 8 shows the values of the integral characteristics for different locations of the insulating plate. Change of kinetic energy, Nusselt number, kinetic energy of turbulent pulsations and energy of temperature pulsations is more convenient to estimate in comparison with Rayleigh-Benard convection, therefore normalized values are given $E_k^* = E_k/E_k^{RBC}$, $Nu^* = Nu/Nu^{RBC}$, $k^* = \langle k \rangle_S / \langle k \rangle_S^{RBC}$ and $k_\theta^* = k_\theta/k_\theta^{RBC}$. Compared to Rayleigh-Benard convection, the kinetic energy decreases from 3% to 16% and the Nusselt number from 1% to 10%. At the same time, the values of kinetic energy and the Nusselt number do not correlate with each other. Thus, a significant restructuring of the flow in the presence of an insulating plate does not necessarily lead to significant changes in the total heat flux, in contrast to its spatial distribution. This can be partially explained by the small size of the plate. The presence of a horizontal plate in the volume strongly affects the integral values of velocity and temperature pulsations. There is both an increase and a decrease in the average kinetic energy of turbulence and the energy of temperature pulsations compared to Rayleigh-Benard convection. The maximum increase of k^* and k_θ^* is 100% and 28%, respectively.

3.3. Convection in the case of a large plate $A=1/2$ (case II)

To answer the question of whether the flow structure and heat transfer are related to the plate size, calculations were performed with a larger plate. A significantly larger plate was chosen as the second option: $A = 1/2$. An increase in the length of the plate by almost three times (up to approximately half of the layer length) leads to expectedly large changes in the temperature distribution (see Figure 9) and flow structure (see Figure 10) compared to a smaller plate. The mean flow in the case of a larger plate consists of two or three convective cells. Even when the plate is centered, the mean flow is asymmetrical. The lack of symmetry may indicate that the flow is not stationary.

Figure 11 shows that in the lower plate position ($y_0 = 1/8$) the blocking of vertical motions leads to a strong suppression of general circulation and convective heat transfer $F_y = \langle w\theta \rangle_t$. As a result, due to the conductive heat flux from the lower boundary, a large part of the area under the plate is heated to a temperature close to the temperature of the lower boundary. It is important to note that when the plate is displaced horizontally, located at a height $y_0 = 1/8$ near to the vertical wall, a weak circulation flow is formed under the plate, but when the plate is exactly in the center, the average circulation is almost absent. At all other locations, there is quite intense asymmetric fluid circulation around the plate. When the plate is placed in the middle of the layer height at both horizontal locations, despite the circulation around the plate, the temperature under the plate is higher and the temperature above it is lower than the average temperature (by about 15-20%).

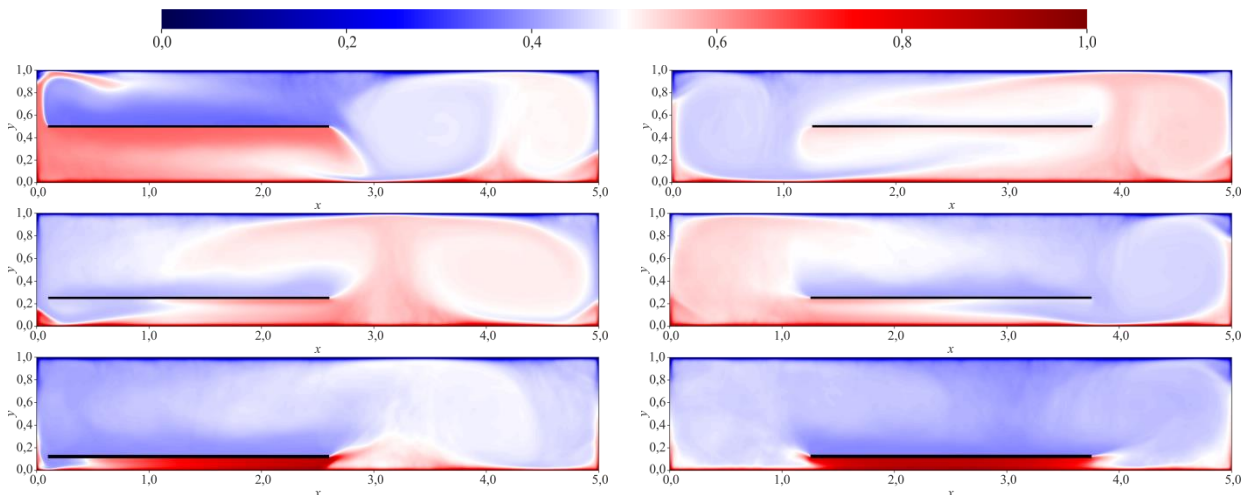


Fig. 9. Average temperature fields at different positions of the thermal insulating plate, $Ra = 3,9 \cdot 10^7$.

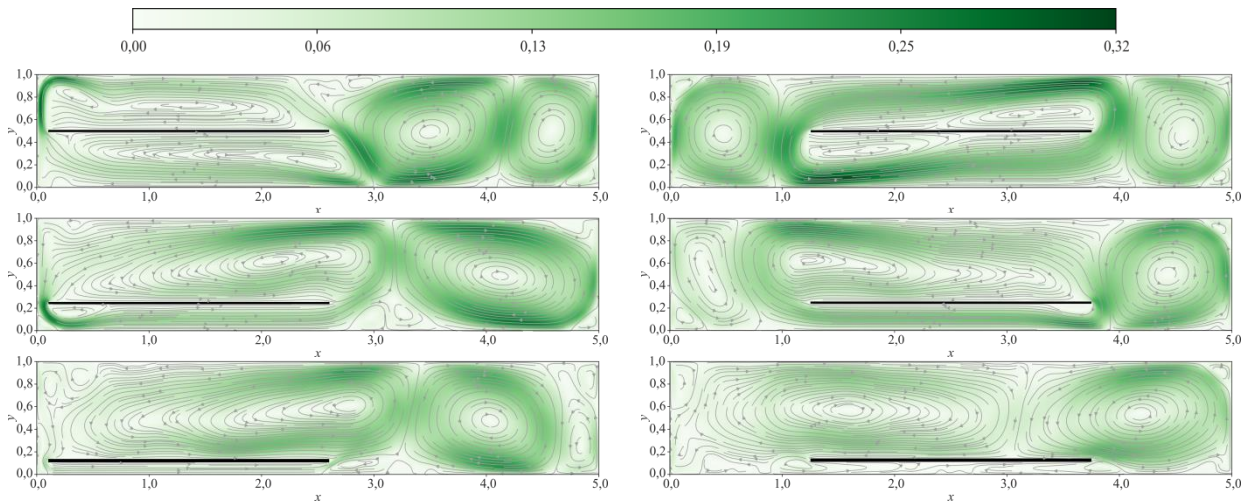


Fig. 10. Structure of the average flow at different positions of the heat insulating plate, $Ra = 3,9 \cdot 10^7$.

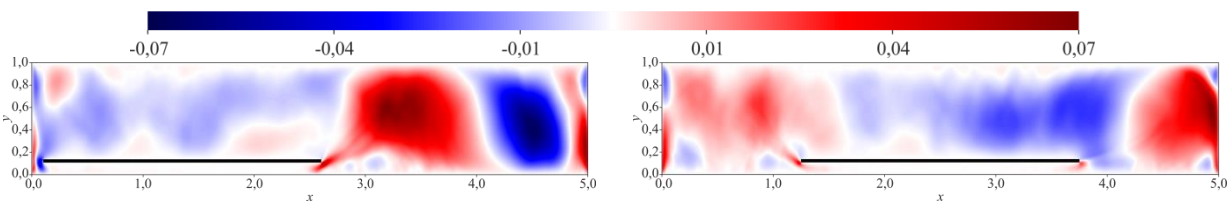


Fig. 11. Convective heat flux F_y distribution at $y_0 = 1/8$, $Ra = 3,9 \cdot 10^7$.

The distribution of temperature and velocity pulsations in the presence of an extended plate is very inhomogeneous (see Figs. 12, 13). It should be noted that, while noticeable temperature pulsations are observed under the plate (at $y_0 = 1/8$ and $y_0 = 1/4$), large velocity pulsations, on the contrary, are characteristic of the region above it (Fig. 13). When the plate is located in the middle height, above and below it, not only significant temperature and velocity pulsations are absent, but also mean flows, i.e. one can speak about the presence of a stagnation zone near the plate.

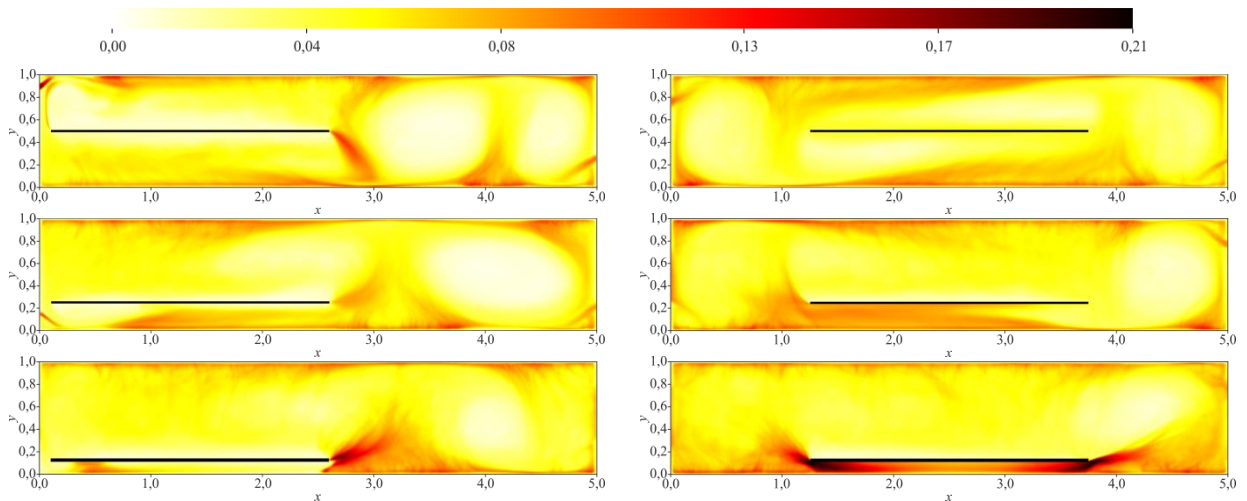


Fig. 12. Distribution of the rms temperature pulsations $\delta\theta_{rms}$ with different location of the heat insulating plate, $Ra = 3,9 \cdot 10^7$.

It is well known that at the moment of flow restructuring, integral characteristics change significantly, so their analysis was performed for quasi-stationary states, in which local small-scale fluctuations of velocity and temperature are possible, but large-scale flow restructuring does not occur (reorientation, suspension, inversion). An analysis of the integral characteristics in the quasi-stationary state showed the following (Fig. 14):

- when the plate is positioned in the middle of the layer (in height), the horizontal displacement significantly affects the mean kinetic energy;
- the central horizontal location leads to a noticeable increase in the kinetic energy, despite the close values of the maximum flow velocity. This is due to the fact that when the plate is close to the side wall, all the main motion is concentrated in the opposite half of the layer;
- in the intermediate case, at $y_0 = 1/4$, the kinetic energy values for both positions are comparable;
- when the plate is displaced even more downward, at $y_0 = 1/8$, the situation changes: the flow acquires more energy when the plate is displaced from the center.

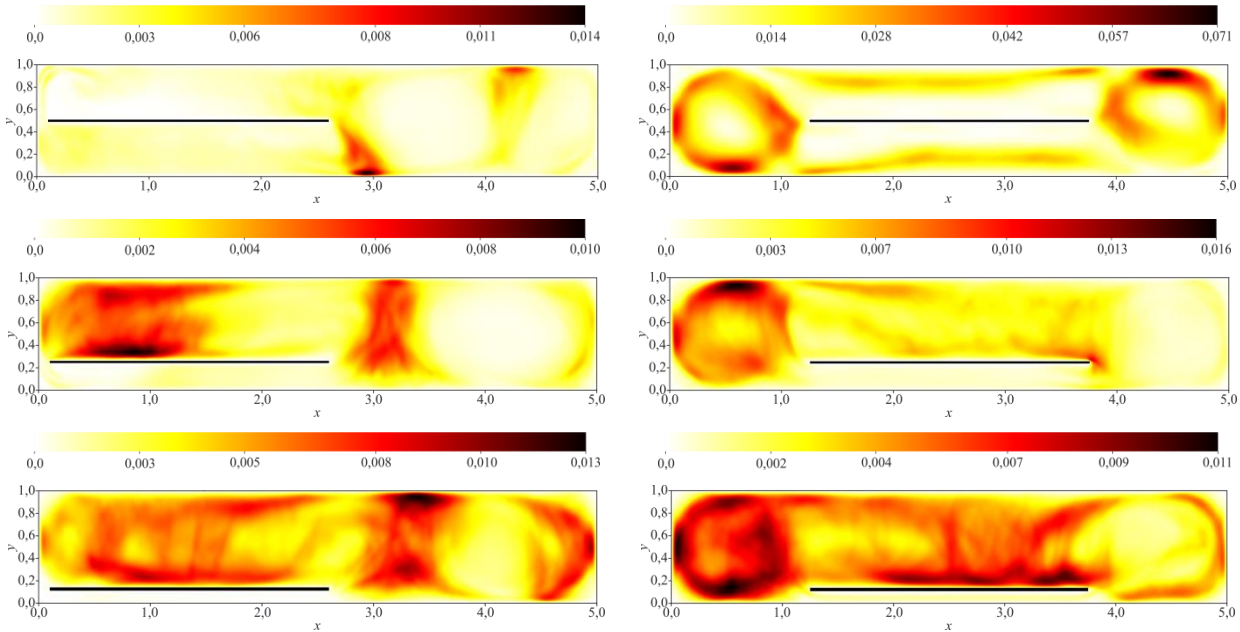


Fig. 13. Distribution of kinetic energy of turbulent pulsations k at different location of the heat insulating plate, $Ra = 3,9 \cdot 10^7$.

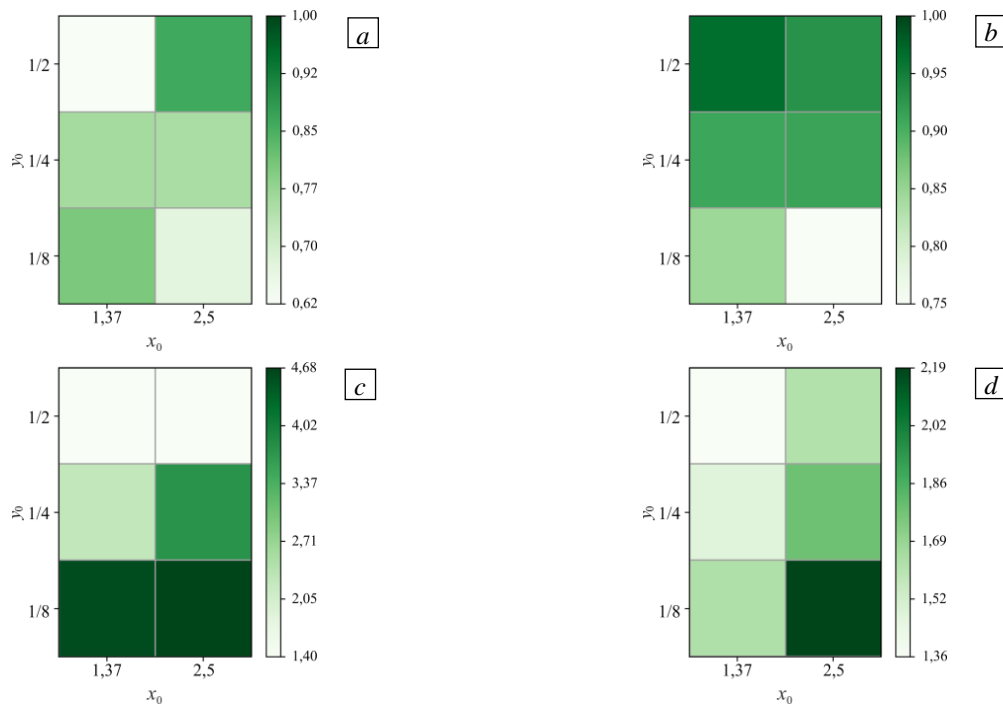


Fig. 14. Normalized integral values for all locations of the heat insulating plate at $Ra = 3,9 \cdot 10^7$: E_k^* (a), Nu_k^* (b), k^* (c) and k_0^* (d).

It should be noted that the presence of the plate has a stronger effect on the pulsations than on the integral characteristics, the level of temperature pulsations and speed pulsations increases significantly, especially at $y_0 = 1/8$.

Before discussing the effect of plate size on convective heat transfer, let us recall that for case I, relatively small changes in the Nusselt number (from 1% to 10%) could be explained by the smallness of the plate itself ($A \approx 1/6$). For case II, the size of the plate is about half the horizontal size of the cavity. Despite this, except for the location of the plate near the lower boundary ($y_0 = 1/8$), the Nusselt number variations are also small (from 3% to 9%). The Nusselt number is determined by the thicknesses of the temperature boundary layers at the upper and lower boundaries. Accordingly, small variations in the Nusselt number indicate that the average boundary layer thicknesses weakly depend on the presence of horizontal plates in the fluid volume in the cavity up to the aspect ratio $A = 1/2$. Since the structure of the flow in the presence of a plate is fundamentally different, we can speak of a weak effect of the flow structure on the thickness of the boundary layer.

The physical interpretation of this effect, which goes counter to intuitive assumptions, can be based on the fact that the thickness of the viscous boundary layer decreases with the Rayleigh number much more slowly than the thickness of the temperature boundary layer [43]. This leads to the fact that the temperature boundary layer gradually becomes thinner than the viscous boundary layer. And since the flow velocity in the viscous boundary layer is small and decreases rapidly toward the wall, the effect of fluid flow on the temperature boundary layer becomes less noticeable as the Rayleigh number increases. As a result, for large values of Rayleigh number (more than 10^6) or the Nusselt number (more than 10), the thickness of the boundary layer is determined mainly by the temperature difference between the isothermal boundaries and the fluid [34, 44], i.e. weakly depends on fluid circulation. Therefore, in the presence of heat-insulating plates in the layer, which significantly affect the flow structure, there is no fundamental change in the average boundary layer thickness. It is important to emphasize that this is valid only under the condition that the distance from the plate to the boundary is significantly greater than the thickness of the boundary layer.

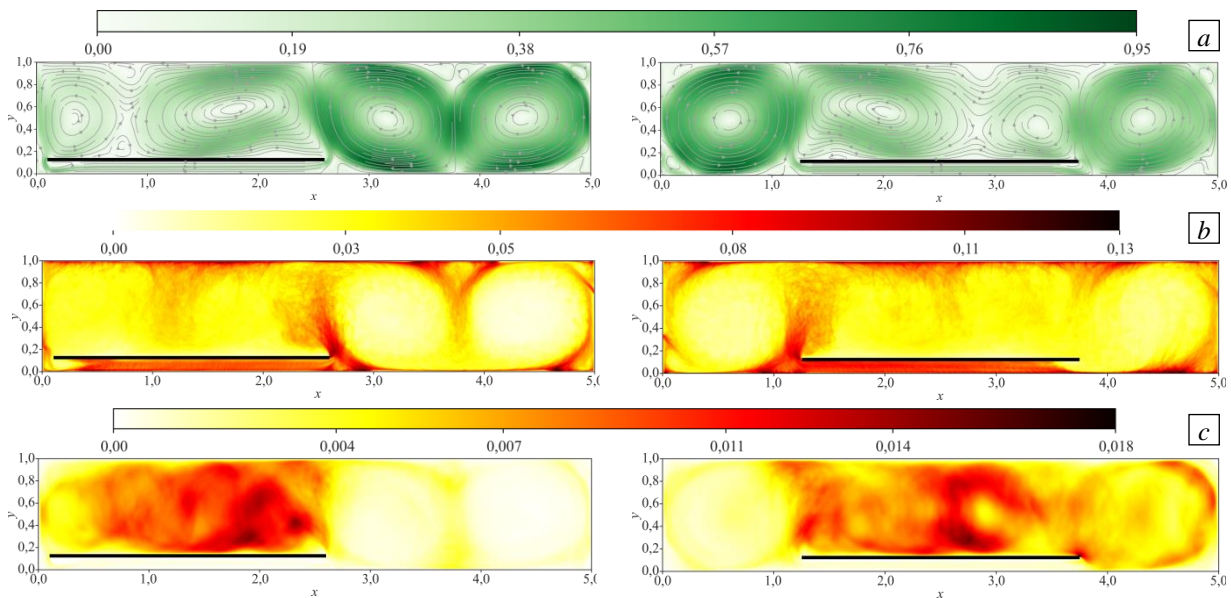


Fig. 15. Mean velocity fields (a), distribution of the rms temperature pulsations $\delta\theta_{\text{rms}}$ (b) and distribution of kinetic energy of turbulent pulsations k (c); $Ra = 3,9 \cdot 10^8$.

The case when the plate is near the lower boundary ($y_0 = 1/8$) requires particular consideration, because, as the plate approaches the boundary layer, it begins to directly affect its structure. If the plate is in the center, then, as noted earlier, fluid motion and convective heat transfer are blocked below it. Due to the conductive heat flux, the liquid layer under the plate heats up to a temperature

close to the boundary temperature. As a result, half of the lower heated boundary is effectively insulated, providing a decrease in the Nusselt number of about 25% compared to Rayleigh-Benard convection. This correlates with a 25% decrease in the total area of the isothermal boundaries, which is not accidental. Previously, a similar result was obtained for mixed boundary conditions at the lower boundary [35, 36], where the change in the Nusselt number was also proportional to the decrease in the total area of the heat exchangers. When the plate is located near the lower boundary, but with the offset to the vertical wall ($x_0 = 1,37, y_0 = 1/8$), a weak mean flow is formed under it, resulting in horizontal heat transfer, and the Nusselt number becomes less than for the Rayleigh-Benard convection by only 15%.

An increase in the Rayleigh number leads to a decrease in the thickness of the temperature boundary layer. Therefore, at a fixed height of the location of the insulating plate, the ratio of this height to the thickness of the boundary layer should increase as the Rayleigh number increases. Accordingly, the influence of the plate position on the structure of the temperature boundary layer should decrease. In order to check this, calculations were performed for a larger value of the Rayleigh number ($Ra = 3,9 \cdot 10^8$) and a fixed plate location height ($y_0 = 1/8$).

Obviously, an increase in the Rayleigh number leads to a visible restructuring of the flow (Fig. 15) and other values of integral characteristics (Table 3). However, the main interest is in the value of heat flux. The obtained results confirm the assumptions made above, that the influence of the heat insulating plate located at a fixed height decreases as the Rayleigh number increases and the thickness of the boundary layers decreases significantly. Thus, while at $Ra = 3,9 \cdot 10^7$ the Nusselt number decreased by 25%, it changed only by 3% at $Ra = 3,9 \cdot 10^8$.

Table 3: Normalized average values of integral characteristics for two positions of the insulating plate for $A = 1/2$ at $Ra = 3,9 \cdot 10^8$.

(x_0, y_0)	Nu^*	E_k^*	k^*	k_θ^*
(1,37, 1/8)	0,97	0,52	4,81	1,32
(2,5, 1/8)	0,97	0,62	3,84	1,47

The Nusselt number is a characteristic of the total heat flux, but in the case of inhomogeneous spatial distribution of the thickness of the temperature boundary layer (and, consequently, of the heat flux), it is useful to consider the spatial distribution of such a heat flux, which can be described by the local Nusselt number Nu_l , which gives an estimate of the local thickness of the boundary layer δ_θ :

$$Nu_l = \frac{\partial \theta}{\partial y} \Big|_{y=0}, \quad \delta_\theta = \frac{1}{2 Nu_l}.$$

Figure 16 shows distributions of the thermal boundary layer thickness along the horizontal coordinate. The average thickness of the thermal boundary layer for Rayleigh-Benard convection at $Ra = 3,9 \cdot 10^7$ is approximately $\delta_\theta = (1/2) Nu \approx 1/40$. Then at $y_0 = 1/8$ the plate is away from the boundary at a distance of five boundary layer thicknesses and has a noticeable effect on it. As the Rayleigh number increases to $Ra = 3,9 \cdot 10^8$, the ratio y_0/δ_θ increases up to 10, and the average boundary layer thickness becomes comparable to that of the boundary layer in Rayleigh-Benard convection. Thus, for the configurations considered, we can conclude that if the value of y_0/δ_θ is of the order of 10 or higher, then an insulating plate, even a sufficiently long one, has no significant effect on the value of the integral heat flux.

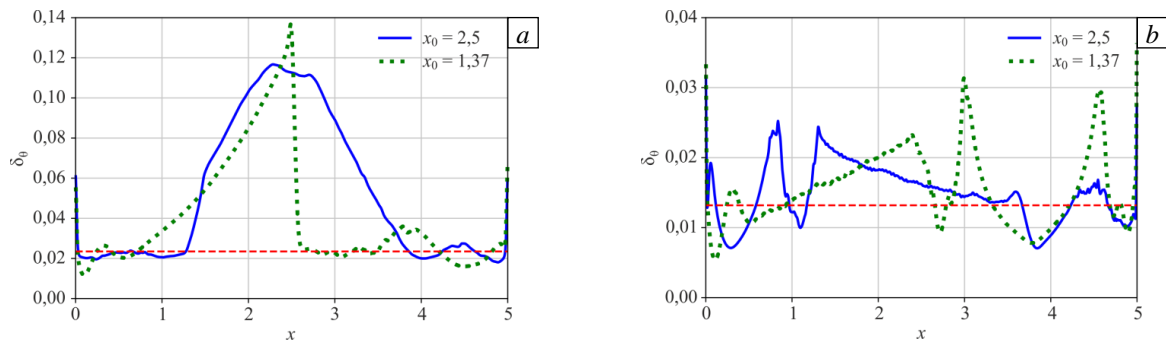


Fig. 16. Distribution of the thermal boundary layer thickness along the axis for $A = 1/2$ at $y_0 = 1/8$: $Ra = 3,9 \cdot 10^7$ (a); $Ra = 3,9 \cdot 10^8$ (b); the dashed line shows the average thickness of the temperature boundary layer for Rayleigh-Benard convection.

4. Conclusion

Based on a numerical study of the influence of a horizontal insulating plate of different size on the structure of convective flows and convective heat transfer in a closed, horizontally stretched cavity, it is shown that even in the case of a relatively small plate ($A = 1/6$), changing its position significantly affects the structure of the flow. Despite the restructuring of the flow, the value of integral convective heat flux changes weakly (not more than 5%). The presence of a larger plate in the layer ($A = 1/2$) and a change in its location leads to greater transformation of the flow structure. Even in this case, however, the changes in the magnitude of the total heat flux, compared to Rayleigh-Benard convection, are relatively small (from 3% to 9%), except for the plate location near the lower boundary ($y_0 = 1/8$), when the Nusselt number decreases by 25%. As the Rayleigh number increases to $Ra = 3,9 \cdot 10^8$, for the fixed location of the plate, the effect of the insulating plate on the heat flux drops sharply. For the system configurations considered, it is concluded that if the ratio of the height of the insulating plate to the thickness of the thermal boundary layer is of the order of 10 or higher, then the insulating plate, even if sufficiently long, has no significant effect on the value of the integral heat flux.

It was shown earlier [38] that the presence of vertical screens in the cavity, leading to a critical restructuring of the flow structure, practically does not change the total heat flux (the Nusselt number). The results obtained in this paper allow us to draw a more general conclusion, namely, that the total heat flow in closed cavities at sufficiently high values of Rayleigh numbers (over 10^6) and Nusselt numbers (over 10), in contrast to the structure of the flow, is weakly dependent on the presence of partitions (vertical or horizontal). However, two important reservations should be made about horizontal plates. First, as stated above, they must be offset from the upper or lower boundary at a distance greater than the thickness of the boundary layer. Otherwise, they thermally insulate the boundary and actually change the boundary conditions. Second, an increase in the size of the horizontal plate results in blocking of vertical motions and vertical heat flux, therefore, starting at a certain size, there will inevitably be a noticeable decrease in the total heat flux.

Acknowledgments. This work was supported by the Russian Foundation for Basic Research and the Perm region within the framework of the scientific project № 20-41-596001. Calculations were performed on the Triton cluster of the Institute of the Russian Academy of Sciences, Ural Branch of the Russian Academy of Sciences, as part of the state program AAAA-A19-119012290101-5.

References

1. Golitsyn G.S. *Prirodnyye protsessy i yavleniya. Volny, planety, konvektsiya, klimat, statistika* [Natural processes and phenomena: Waves, planets, convection, climate, and statistics]. Moscow, Fizmatlit, 2004. 344 p.

2. Bergman T.L., Lavine A.S., Incropera F., DeWitt D.P. *Fundamentals of heat and mass transfer*. John Wiley & Sons, 2011. 1080 p.
3. Gershuni G.Z., Zhukhovitskii E.M. *Convective instability of incompressible fluids*. Keter Publishing House, 1976. 330 pp.
4. Gershuni G.Z., Zhukhovitskiy E.M., Nepomnyashchiy A.A. *Ustoychivost' konvektivnykh techeniy* [Stability of convective flows]. Moscow, Nauka, 1989. 320 p.
5. Getling A.V. *Konveksiya Reyleya-Benara. Struktury i dinamika*. [Rayleigh–Bénard convection. Structure and dynamics]. Moscow, Editorial URSS, 1999. 248 c.
6. Lappa M. *Thermal convection: Patterns, evolution and stability*. John Wiley & Sons, 2009. 670 p. <https://doi.org/10.1002/9780470749982>
7. Verma M.K. *Physics of buoyant flows: From instabilities to turbulence*. World Scientific, 2018. 352 p. <https://doi.org/10.1142/10928>
8. Schubert G., Turcotte D. L., Olson P. *Mantle convection in the Earth and planets*. Cambridge University Press, 2001. 940 p. <https://doi.org/10.1017/CBO9780511612879>
9. Gurnis M. Large-scale mantle convection and the aggregation and dispersal of supercontinents. *Nature*, 1988, vol. 332, pp. 695-699. <https://doi.org/10.1038/332695a0>
10. Lowman J.P., Jarvis G.T. Mantle convection models of continental collision and breakup incorporating finite thickness plates. *Phys. Earth Planet. Inter.*, 1995, vol. 88, pp. 53-68. [https://doi.org/10.1016/0031-9201\(94\)05076-A](https://doi.org/10.1016/0031-9201(94)05076-A)
11. King S.D., Lowman J.P., Gable C.W. Episodic tectonic plate reorganizations driven by mantle convection. *Earth Planet. Sci. Lett.*, 2002, vol. 203, pp. 83-91. [https://doi.org/10.1016/S0012-821X\(02\)00852-X](https://doi.org/10.1016/S0012-821X(02)00852-X)
12. Lowman J.P., King S.D., Trim S.J. The influence of plate boundary motion on planform in viscously stratified mantle convection models. *J. Geophys. Res.*, 2011, vol. 116, B12402. <https://doi.org/10.1029/2011JB008362>
13. Heron P.J., Lowman J.P., Stein C. Influences on the positioning of mantle plumes following supercontinent formation. *J. Geophys. Res. Solid Earth*, 2015, vol. 120, pp. 3628-3648. <https://doi.org/10.1002/2014JB011727>
14. Trubitsyn V.P. Principles of the tectonics of floating continents. *Izv. Phys. Solid Earth.*, 2000, vol. 36, no. 9, pp. 708-741.
15. Trubitsyn V., Kaban M., Mooney W., Reigber C., Schwintzer P. Simulation of active tectonic processes for a convecting mantle with moving continents. *Geophys. J. Int.*, 2006, vol. 164, pp. 611-623. <https://doi.org/10.1111/j.1365-246X.2006.02832.x>
16. Bobrov A.M. Numerical modeling of the distribution of horizontal stresses in a moving continental plate. *Izv. Phys. Solid Earth.*, 2010, vol. 6, pp. 477-485. <https://doi.org/10.1134/S1069351310060029>
17. Trubitsyn V.P. Problems of global geodynamics. *Izv. Phys. Solid Earth.*, 2019, vol. 55, pp. 152-167. <https://doi.org/10.1134/S1069351319010129>
18. Kirdyashkin A.A., Dobretsov N.L., Kirdyashkin A.G. Experimental modeling of the influence of subduction on the spatial structure of convection currents in the asthenosphere under continents. *Dokl. Earth Sci.*, 2002, vol. 385, no. 5, pp. 546-550.
19. Kirdyashkin A.A., Kirdyashkin A.G., Surkov N.V. Thermal gravitational convection in the asthenosphere beneath a mid-oceanic ridge and stability of main deep-seated parageneses. *Geologiya i geofizika – Russian Geology and Geophysics*, 2006, vol. 47, no. 1, pp. 76-94.
20. Kirdyashkin A.A., Kirdyashkin A.G. Effect of the oceanic lithosphere velocity on free convection in the asthenosphere beneath mid-ocean ridges. *Izv. Phys. Solid Earth.*, 2008, vol. 44, pp. 291-302. <https://doi.org/10.1134/s11486-008-4003-5>
21. Zhang J., Libchaber A. Periodic boundary motion in thermal turbulence. *Phys. Rev. Lett.*, 2000, vol. 84, 4361. <https://doi.org/10.1103/PhysRevLett.84.4361>
22. Popova E.N., Frick P.G. Large-scale flows in a turbulent convective layer with an immersed moving thermal insulator. *Fluid Dyn.*, 2003, vol. 38, pp. 862-867. <https://doi.org/10.1023/B:FLUI.0000015226.47864.b8>
23. Zhong J.Q., Zhang J. Thermal convection with a freely moving top boundary. *Phys. Fluid.*, 2005, vol. 17, 115105. <https://doi.org/10.1063/1.2131924>
24. Zhong J.Q., Zhang J. Dynamical states of a mobile heat blanket on a thermally convecting fluid. *Phys. Rev. E*, 2007, vol. 75, 055301. <https://doi.org/10.1103/PhysRevE.75.055301>
25. Zhong J.Q., Zhang J. Modeling the dynamics of a free boundary on turbulent thermal convection. *Phys. Rev. E*, 2007, vol. 76, 016307. <https://doi.org/10.1103/PhysRevE.76.016307>

26. Liu B., Zhang J. Self-induced cyclic reorganization of free bodies through thermal convection. *Phys. Rev. Lett.*, 2008, vol. 100, 244501. <https://doi.org/10.1103/PhysRevLett.100.244501>
27. Mao Y., Zhong J.Q., Zhang J. The dynamics of an insulating plate over a thermally convecting fluid and its implication for continent movement over convective mantle. *J. Fluid Mech.*, 2019, vol. 868, pp. 286-315. <https://doi.org/10.1017/jfm.2019.189>
28. Whitehead J.A., Shea E., Behn M.D. Cellular convection in a chamber with a warm surface raft. *Phys. Fluid.*, 2011, vol. 23, 104103. <https://doi.org/10.1063/1.3651341>
29. Whitehead J.A., Behn M.D. The continental drift convection cell. *Geophys. Res. Lett.*, 2015, vol. 42, pp. 4301-4308. <https://doi.org/10.1002/2015GL064480>
30. Wang F., Huang S.D., Xia K.Q. Thermal convection with mixed thermal boundary conditions: effects of insulating lids at the top. *J. Fluid Mech.*, 2017, vol. 817, R1. <https://doi.org/10.1017/jfm.2017.121>
31. Ripesi P., Biferale L., Sbragaglia M., Wirth A. Natural convection with mixed insulating and conducting boundary conditions: low- and high-Rayleigh-number regimes. *J. Fluid Mech.*, 2014, vol. 742, pp. 636-663. <https://doi.org/10.1017/jfm.2013.671>
32. Bakhuis D., Ostilla-Mónico R., van der Poel E.P., Verzicco R., Lohse D. Mixed insulating and conducting thermal boundary conditions in Rayleigh-Bénard convection. *J. Fluid Mech.*, 2018, vol. 835, pp. 491-511. <https://doi.org/10.1017/jfm.2017.737>
33. Evgrafova A., Sukhanovskii A. Specifics of heat flux from localized heater in a cylindrical layer. *Int. J. Heat Mass Tran.*, 2019, vol. 135, pp. 761-768. <https://doi.org/10.1016/j.ijheatmasstransfer.2019.02.038>
34. Sukhanovskii A., Evgrafova A. Dependence of boundary layer thickness on layer height for extended localised heaters. *Exp. Therm. Fluid Sci.*, 2021, vol. 121, 110275. <https://doi.org/10.1016/j.expthermflusci.2020.110275>
35. Vasiliev A.Yu., Sukhanovskii A.N., Stepanov R.A. Convective turbulence in a cubic cavity under nonuniform heating of a lower boundary. *J. Appl. Mech. Tech. Phy.*, 2020, vol. 61, pp. 1049-1058. <https://doi.org/10.1134/S0021894420070172>
36. Vasiliev A., Sukhanovskii A. Turbulent convection in a cube with mixed thermal boundary conditions: low Rayleigh number regime. *Int. J. Heat Mass Tran.*, 2021, vol. 174, 121290. <https://doi.org/10.1016/j.ijheatmasstransfer.2021.121290>
37. Nandukumar Y., Chakraborty S., Verma M.K., Lakkaraju R. On heat transport and energy partition in thermal convection with mixed boundary conditions. *Phys. Fluid.*, 2019, vol. 31, 066601. <https://doi.org/10.1063/1.5095242>
38. Ciliberto S., Cioni S., Laroche C. Large-scale flow properties of turbulent thermal convection. *Phys. Rev. E*, 1996, vol. 54, R5901. <https://doi.org/10.1103/PhysRevE.54.R5901>
39. Shishkina O., Stevens R.J.A.M., Grossmann S., Lohse D. Boundary layer structure in turbulent thermal convection and its consequence for the required numerical resolution. *New J. Phys.*, 2010, vol. 12, 075022. <https://doi.org/10.1088/1367-2630/12/7/075022>
40. Wagner S., Shishkina O. Aspect-ratio dependency of Rayleigh-Bénard convection in box-shaped containers. *Phys. Fluid.*, 2013, vol. 25, 085110. <https://doi.org/10.1063/1.4819141>
41. Soucasse L., Podvin B., Rivière P., Soufiani A. Proper orthogonal decomposition analysis and modelling of large-scale flow reorientations in a cubic Rayleigh-Bénard cell. *J. Fluid Mech.*, 2019, vol. 881, pp. 23-50. <https://doi.org/10.1017/jfm.2019.746>
42. Xu A., Chen X., Xi H.D. Tristable flow states and reversal of the large-scale circulation in two-dimensional circular convection cells. *J. Fluid Mech.*, 2021, vol. 910, A33. <https://doi.org/10.1017/jfm.2020.964>
43. Xia K.Q. Current trends and future directions in turbulent thermal convection. *Theor. Appl. Mech. Lett.*, 2013, vol. 3, 052001. <https://doi.org/10.1063/2.1305201>
44. Golitsyn G.S. Simple theoretical and experimental study of convection with some geophysical applications and analogies. *J. Fluid Mech.*, 1979, vol. 95, pp. 567-608. <https://doi.org/10.1017/S0022112079001609>

The authors declare no conflict of interests.

The paper was submitted 26.10.2021; approved after reviewing 28.12.2021; accepted for publication 24.02.2022